J Mol Model (2013) 19:727–735
DOI 10.1007/s00894-012-1586-x

ORIGINAL PAPER

QM study and conformational analysis of an isatin Schiff base as a potential cytotoxic agent

Ramin Miri · Nima Razzaghi-asl · Mohammad K. Mohammadi

Received: 12 July 2012 / Accepted: 28 August 2012 / Published online: 29 September 2012

Abstract Isatin is an important compound from the biological aspect of view. It is an endogenous substance and moreover; various pharmacological activities have been reported for isatin and its derivatives. In-vitro cytotoxic effects of the prepared isatin Schiff bases toward HeLa, LS180 and Raji human cancer cell lines has been reported in our previous work. 3-(2-(4-nitrophenyl)hydrazono) indolin-2-one was found to be the most potent one among the studied compounds (IC_{30}=12.2 and 21.8 μM in HeLa and LS-180 cell lines, respectively). Obtained biological data could be well interpreted using docking binding energies toward vascular endothelial growth factor receptor (VEGFR-2); a key anticancer target being biologically investigated against various isatin derivatives. In the present work, quantum mechanical (QM) method including functional B3LYP in association with split valence basis set using polarization functions (Def2-SVP) was used to estimate individual ligand-residue interaction energies for the docked 3-(2-(4-nitrophenyl)hydrazono) indolin-2-one into VEGFR-2 active site. Results were further interpreted via calculated polarization effects induced by individual amino acids of the receptor active site. A fairly good correlation could be found between polarization effects and estimated binding energies (R^2=0.7227). Conformational analysis revealed that 3-(2-(4-nitrophenyl) hydrazono) indolin-2-one might not necessarily interact with the VEGFR-2 active site in its minimum energy conformation.

Keywords B3LYP · Conformational analysis · Cytotoxicity · Isatin · Quantum mechanical

R. Miri · N. Razzaghi-asl
Medicinal and Natural Products Chemistry Research Center,
Shiraz University of Medical Sciences,
3288-71345 Shiraz, Iran

R. Miri · N. Razzaghi-asl
Department of Medicinal Chemistry, School of Pharmacy,
Shiraz University of Medical Sciences,
Shiraz, Iran

M. K. Mohammadi (✉)
Faculty of Sciences, Ahvaz Branch, Islamic Azad University,
Ahvaz, Iran
e-mail: mohammadi@iauahvaz.ac.ir

Introduction

Isatin is a natural product found in a number of plants including those of the genus *Isatis* [1]. It has also been found as a metabolic derivative of adrenaline in humans [2]. Moreover, it has been demonstrated that isatin is found at higher levels in patients involved with neuropathological conditions and also proved to be a competitive MAO-B inhibitor [3, 4]. Various derivatives of isatin are known to possess a range of pharmacological properties including antiprotozoal [5, 6], antiglycation [7], anticonvulsant and sedative-hypnotic [8, 9], anti-inflammatory [10], antibacterial and anti-fungal [11] activities. Thus isatin is a biologically validated starting point for the design and synthesis of chemical libraries directed at these targets [12]. Due to the privileged nature of isatin, libraries designed and synthesized around the basic structure of this scaffold may yield medicinally active compounds with high hit rates.

In a typical lead/drug discovery protocol, potential candidate molecules may suffer from undesirable properties in their pharmacokinetic and pharmacodynamic profiles. Structure-based drug design has been considered as one of the major strategies in achieving potential drug candidates [13, 14]. In lead-drug development strategies, combination of experimental methods with computer aided molecular design (CAMD) techniques is essential for the development of new drugs aimed at new targets, and thus for medicinal chemistry [15].

A variety of computational chemistry methods are available for running CAMD projects. These methods can be divided into two categories; ligand-based and structure-based methods. Within this scenario, theoretical methods based on density-functional theory (DFT) are going to play an increasingly important role in many applications of computational chemistry to drug discovery [16–18]. One of the most used DFT methods is Becke three-parameter Lee-Yang-Parr (B3LYP) hybrid density functional theory [19]. This technique has been applied for conformational analysis of some cytotoxic agents [20].

A number of isatin based chemical structures have been reported to exhibit cytotoxic activity [21–24] and moreover inhibitory activity of 3-substituted-indolin-2-ones against VEGFR-2 have been demonstrated elsewhere [25]. VEGFR-2 is a cell surface receptor for vascular endothelial growth factors and is involved in cell proliferation/angiogenesis [26–28]. In light of the above information and in continuation of our work [29], VEGFR-2 was chosen as target for our theoretical studies. B3LYP level of theory supplemented with the Def2-SVP as split basis set using polarization functions [30] was applied to calculate the individual ligand-amino acid binding energies for 3-(2-(4-nitrophenyl) hydrazono) indolin-2-one as the most potent cytotoxic isatin derivative in our studies (IC_{30}=12.2 and 21.8 μM in HeLa and LS-180 cell lines, respectively) [29]. Estimating the proportion of individual amino acid-ligand interaction energies in total binding energy would be a very useful trend in pharmacophore discernment and development (amino acid decomposition analysis). Comparative conformational analysis of the ligand structures in the optimized and docked conformers were performed using the same basis set. No such report could be found for studied isatins with VEGFR-2.

Experimental

Computational section

X-ray crystal structure of VEGFR-2 was obtained from the Brookhaven protein data bank (2OH4; http://www.pdb.org/). Cognate ligand and all crystallographic water molecules were removed from receptor structure. All the pre-processing steps for receptor structure were performed via WHAT IF server (European Molecular Laboratory Heidelberg, Germany) and AutoDock Tools 1.5.4 program (ADT) which has been released as an extension suite to the Python Molecular Viewer [31]. All the molecular images were produced using VMD program [32].

Schematic 2D representations of the ligand-receptor binding maps for 3-(2-(4-nitrophenyl) hydrazono) indolin-2-one/VEGFR-2 complex were generated using LIGPLOT [33]. For this purpose, all involved amino acids (residues) were considered in their real electrostatic state. In each residue under study, N-terminal was acetylated and C-terminal was methyl amidated to mimic the original electron density. All conformational and configurational features were held as X-ray structure. The position of hydrogen bonds are not clearly recognized in a typical X-ray crystallographic file, and due to this limitation, we further optimized the heavy atom-hydrogen bonds by semi-empirical PM3 method using heavy atom fixing approximation (constrained optimizations) [34]. All the interaction energies were estimated by B3LYP/Def2-SVP method. All calculations were done with the ORCA quantum chemistry package [19].

Results and discussion

Ligand-receptor interactions

Previously we have found that top ranked AutoDock-based binding energies ($kcal\,mol^{-1}$) for docked arylhydrazono/arylimino indolin-2-one systems into VEGFR-2 active site were in adaptable correlation with the in-vitro cytotoxicity data. Moreover, docking results were supported almost by high cluster populations. Among prepared compounds, 3-(2-(4-nitrophenyl) hydrazono) indolin-2-one was selected as a model for QM analysis due to its higher potency in in-vitro cytotoxicity assays. For 3-(2-(4-nitrophenyl) hydrazono) indolin-2-one, IC_{30} values were found to be 12.2 and 21.8 μM in HeLa and LS-180 cell lines, respectively [29].

Molecular docking is a popular method for attaining ligand-receptor binding patterns, but with all of its advantageous features, docking simulation provides no information on individual ligand-amino acid binding energies in the active-site of the receptor. The contribution of each amino acid to the total ligand-receptor binding energy is of significant importance in pharmacophore design and development. We were convinced to estimate the binding energies of a 3-(2-(4-nitrophenyl) hydrazono) indolin-2-one with individual residues of the VEGFR-2 active site. For this purpose, a model system including eight amino acids of the VEGFR-2 active site was constructed (Fig. 1). The evaluated residues (Leu838, Val914, Glu915, Asn921, Leu1o33, Leu30, Phe1045, and Arg1049) were selected on the basis of constructed binding pattern for 3-(2-(4-nitrophenyl) hydrazono) indolin-2-one/VEGFR-2 complex [29].

Ligand-amino acid systems were subjected to optimization process with the same basis set to obtain the exact geometry of H-bonds (Table 1). Hydrogen bond geometries were described as H-donor-acceptor angles. It should be noted that hydrogen bond lengths were obtained considering H…acceptor distances.

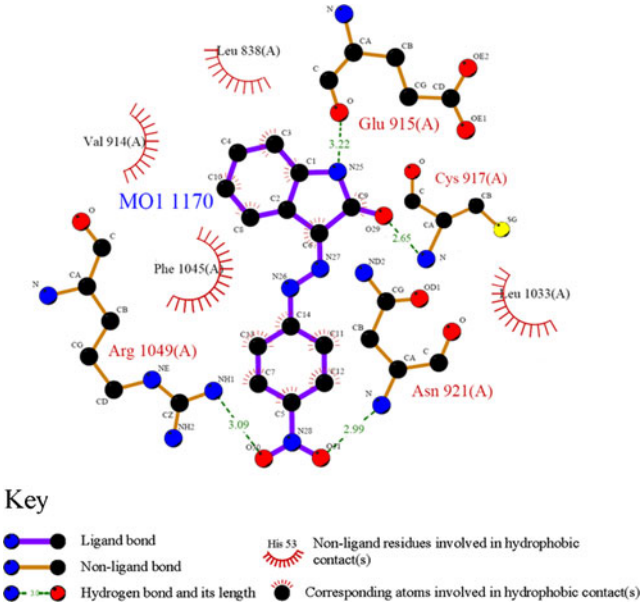

Fig. 1 2D scheme of interactions between docked 3-(2-(4-nitrophenyl) hydrazono) indolin-2-one and active site of VEGFR-2 generated by LIGPLOT, PBD deposition code: 2OH4

Ligand-residue binding energies (ΔE_b) were calculated using Eq. 1.

$$\Delta E = E_{L-R} - E_R - E_L \quad (1)$$

$E_{L\text{-}R}$ stands for residue ligand interaction energy. E_R and E_L indicate the electronic energies for residues and ligand, respectively. Regarding this, various binding energies between 3-(2-(4-nitrophenyl) hydrazono) indolin-2-one and key residues surrounding the active site of VEGFR-2 were obtained independently. The relevant data are shown in Table 2.

Our results demonstrated that hydrogen bonding interactions are of significant importance in overall binding of 3-(2-(4-nitrophenyl) hydrazono) indolin-2-one to its target. One of the key interactions was detected in the case of Arg1049 for which a tight binding (−12.13 kcal mol^{-1}) to the ligand occurred. The estimated bonding energy could be well interpreted considering a charge-assisted electrostatic attraction between oxygen atom

Table 1 Hydrogen bond distances (Å) for docked inhibitor [3-(2-(4-nitrophenyl) hydrazono) indolin-2-one] into VEGFR-2 active site (PDB deposition code: 2OH4)

Participant amino acids[a]	No. of H-bonds	Optimized hydrogen bond distances (Å) state	Hydrogen bond angle (degree)
Glu915	1	2.98	53.89
Cys917	1	2.56	27.52
Asn921	1	2.27	36.35
Arg1049	1	2.12	10.11

[a] For detailed participant atoms, readers are referred to Fig. 1

Table 2 Binding energies between residues of VEGFR-2 active site and docked 3-(2-(4-nitrophenyl) hydrazono) indolin-2-one

Residues	Binding energy (kcal/mol)
Arg1049	−12.13
Asn921	−8.29
Cys917	−0.46
Phe1045	−1.30
Val914	1.23
Glu915	−5.43
Leu838	−0.96
Leu1033	−0.38
Estimated total binding energy	−27.72

of nitro group in ligand (4-NO_2-Ph) and guanine moiety of Arg1049 (Fig. 1). In Asn921, the charge-assisted electrostatic interaction might not be detected in obtained binding pattern, but noticeable binding energy (−8.29 kcal mol^{-1}) emphasized us to take into account hydrophobic interactions as well as H-bonding with nitro oxygen atom (O31) of ligand. This hydrophobic interaction may be observed between carbon chain of Asn921 and phenyl (4-NO_2-Ph) moity of the ligand.

According to the above results, it may be supposed that *para*-nitro group of phenyl moiety in the 3-(2-(4-nitrophenyl) hydrazono) indolin-2-one structure may serve as an efficient hydrogen acceptor site for making key H-bonds with residues of the VEGFR-2. Glu915-ligand hydrogen bonding might be supported with about −5 kcal mol^{-1} energy (Table 2). However, higher binding energies might be expected for this interaction if carboxyl group of the Glu915 residue participated in charge-assisted H-bonding. In the case of Cys917, the estimated binding energy (−0.46 kcal mol^{-1}) may be interpreted in the following ways:

- The electrostatic attraction between N-terminal of Cys917 and oxygen atom (O29) of indolin-2-one carbonyl group may be penalized by repulsive hydrophobic interactions of Cys917 with ligand.
- Weaker H-bonding between Cys917 and ligand could be attributed to the inappropriate geometrical pose of donor/acceptor groups which is very determinative in achieving tight bonds. The estimated angle for H-bond (Cys917 NH- indolin O29) was 27.52º (Fig. 2). H-bond distance (H….acceptor) was also found to be 2.56 Å (Table 1).

Our calculations indicated that hydrophobic contact between ligand and Val914 residue is repulsive and on the basis of hydrophobic interaction map, this may be attributed to the close contacts of Val914 with C3 and C14 atoms of an indolin-2-one ring (Fig. 3). This interaction term has a weakening effect on total binding energy to the receptor (Table 2).

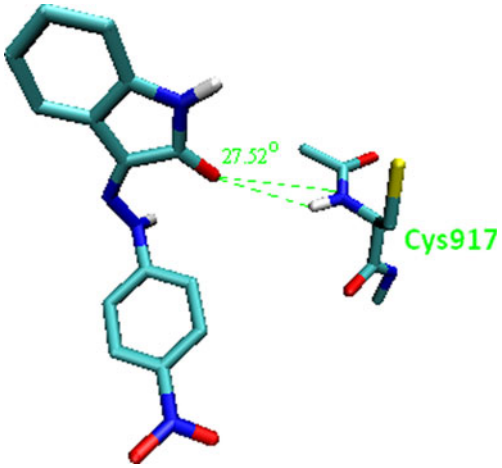

Fig. 2 H-bond angle for donor/acceptor participants in Cys917 residue of VEGFR-2 and docked 3-(2-(4-nitrophenyl) hydrazono) indolin-2-one

Phe1045 contributed to the possible π-π stacking interactions with phenyl ring (4-NO_2-Ph) of the ligand and our calculations assigned a −1.30 kcal mol^{-1} binding energy to this hydrophobic contact (Table 2). Other hydrophobic contacts could be observed for Leu838 and Leu1033 with C13 and C12-C11 atoms of the phenyl ring (4-NO_2-Ph), respectively. C9 atom of indolin-2-one also contributed to non-bonded interactions with Leu1033 (Fig. 3). It should be noted that

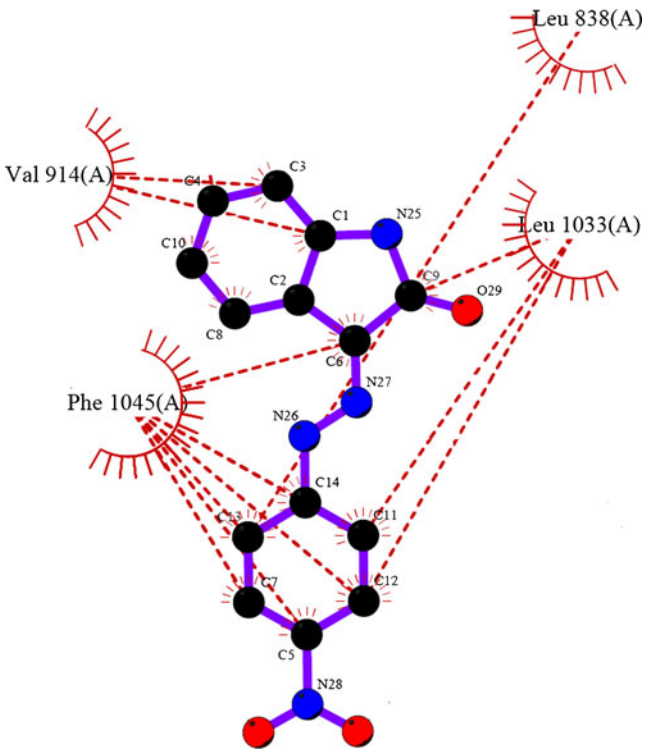

Fig. 3 2D scheme of hydrophobic binding map between docked 3-(2-(4-nitrophenyl) hydrazono)indolin-2-one and active site of VEGFR-2 generated by LIGPLOT, PBD deposition code: 2OH4

hydrophobic interactions are complex in nature and their treatment in a single model would face some shortcomings, but from the least point of view, active site oriented pose of the ligand may be analyzed.

According to the ligand-receptor binding profile (Fig. 1) it may be assumed that hydrazine linker (N26-N27) may not be involved directly in bonding interactions with the amino acids of the VEGFR-2 active site, but a directivity effect toward proper orientation of 3-(2-(4-nitrophenyl) hydrazono) indolin-2-one in the binding pocket of the receptor may be considered for this linker group.

Induced polarizability

Stereoelectronic effects are very important in evaluation of ligand-receptor interactions. Ligand electronic structure may address its orientation in the enzyme active site and significant inhibitory activity would be expected provided that complementary fitness of the ligand and electronic surfaces of the receptor occurs. A part of stereoelectronic effect could be considered as ligand polarizability induced by various residues of the active site. This principal concept can be considered via assigning Mulliken partial charges to the heavy atoms of the ligand in the active site of the receptor [35]. Considering the above important features and with the aim of analyzing obtained individual ligand-residue binding energies in a more detailed manner, we calculated the inducing effect of each involved amino acid on docked ligand.

Ligand polarizability can be defined as the difference between sum of squared partial charges in the bound and unbound states which may be defined as Δq^2. The larger induced polarizability value is indicative of higher participation of electrostatic interactions in binding of amino acid to the ligand. The relevant induced polarization effects are summarized in Table 3.

Table 3 Sum of squared Mulliken charges for 3-(2-(4-nitrophenyl) hydrazono) indolin-2-one induced by various residues of VEGFR-2 active site

Inducing amino acid	q^{2a}	$\Delta(q^2)^b$
Arg1049	0.841	0.925
Asn921	0.848	0.918
Cys917	0.858	0.908
Phe1045	0.867	0.899
Val914	0.854	0.889
Glu915	0.851	0.916
Leu838	0.885	0.891
Leu1033	0.874	0.892

[a] Sum of squared partial charges in bound ligand

[b] (sum of squared partial charges in optimized ligand – sum of squared partial charges in docked ligand)

Our DFT based calculations showed a good correlation between estimated binding energies and induced polarizability in the case of amino acids making H-bonds with receptor:

Binding energy: Arg1049>Asn921>Glu915>Cys917
Induced polarizability: Arg1049>Asn921>Glu915>Cys917

Hydrophobic forces are also electrostatic in nature since they are caused by correlations in the fluctuating polarizations of nearby particles. Considering this, a fairly good polarization effect of Cys917 may be explainable.

Our estimation showed that among residues of VEGFR-2 active site, Arg1049 and Asn921 had the largest polarization effect on 3-(2-(4-nitrophenyl) hydrazono) indolin-2-one. This result was in accordance with our calculated binding energies (Table 2). Another considerable feature could be observed for Leu1033 which has been found to have lower inducing effect on ligand structure. This finding was almost in accordance with calculated Leu1033-ligand hydrophobic binding energy (Table 2).

A typical ligand-residue interaction may consist of several forces with varied electrostatic natures (hydrogen-bonding and hydrophobic contacts). This complexity makes it difficult to correlate induced polarizations to binding patterns. Possible correlation of polarization effects (Table 3) to the binding energies of ligand (Table 2) was evaluated via plotting the regression curve of individual ligand-residue binding energies versus induced charges (Fig. 4). Interestingly a fairly good correlation coefficient (R^2=0.7227) was achieved. These results confirmed that larger polarization effects occurred for amino acids being involved in key electrostatic interactions.

Conformational analysis

The difference between ligand electronic energies in the optimized and docked conformers (E_L) may be indicative of ligand conformational instability upon binding to the receptor. Bearing this in mind, we decided to model the conformational change of 3-(2-(4-nitrophenyl) hydrazono) indolin-2-one while binding to the active site of VEGFR-2. Aqueous biological medium was modeled in our ligand optimization procedure. The imposed conformational deviation of ligand might be observed in Fig. 5.

Different energies of the evaluated ligand conformations may be a direct outcome of varied internal energies of ligand in its docked and optimized conditions within biological media ($\Delta E_{instability}$). $\Delta E_{inst.}$ needs to be considered in order to adjust obtained binding energies. For the purpose of calculating $\Delta E_{inst.}$, optimized structural conformations of 3-(2-(4-nitrophenyl) hydrazono) indolin-2-one was obtained in water and relevant energy was assigned to this free state. $\Delta E_{inst.}$ may be well related with the free energy of binding via following equations:

$$\Delta G_b = \Delta H_b - T\Delta S_b \quad (2)$$

$$\Delta H_b = \Delta E_t - P\Delta V \approx \Delta E_{tb} \quad (3)$$

$$\Delta E_{tb} = \Delta E_b + \Delta E_{inst.} \quad (4)$$

Higher $\Delta E_{inst.}$ values support more positive total binding energies (ΔE_{tb}). This would consequently lead to weaker ligand-receptor interactions (ΔG_b). Our calculation revealed that 3-(2-(4-nitrophenyl) hydrazono) indolin-2-one gained 29.05 kcalmol^{-1} conformational instability upon binding to the VEGFR-2. This may be indicative of a noticeable conformational shift toward less stable geometric pose. It seemed that functional groups being involved in key interactions with receptor, exhibited higher conformational changes. These outcomes demonstrated that 3-(2-(4-nitrophenyl) hydrazono) indolin-2-one might not necessarily interact with the active site of VEGFR-2 in its minimum energy conformation.

For further structural investigations, optimized 3D structure of 3-(2-(4-nitrophenyl) hydrazono) indolin-2-one was obtained by DFT calculations via B3LYP method in association with split valence basis set using polarization functions (Def2-SVP). The resulted geometric parameters in terms of bond lengths and dihedral angles are summarized in Tables 4 and 5. All the bond lengths of the DFT optimized structure were in good correlation with crystallographic data.

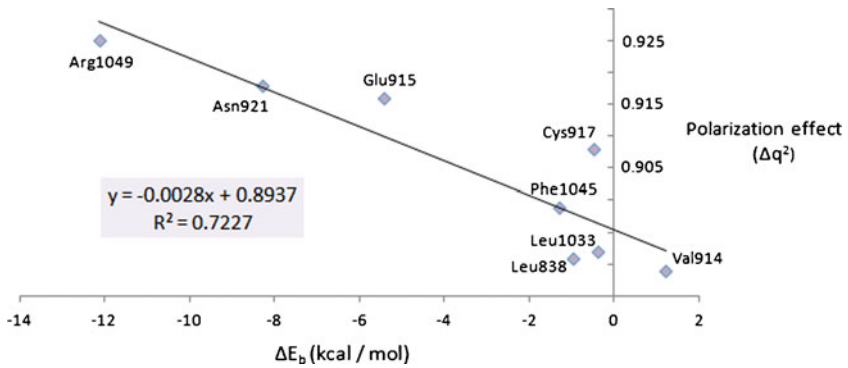

Fig. 4 Correlation curve of induced polarization effects versus ligand-amino acid binding energies for docked 3-(2-(4-nitrophenyl) hydrazono) indolin-2-one into VEGFR-2 active site (PDB code: 2OH4), (Δq^2: sum of squared partial charges in optimized ligand – sum of squared partial charges in docked ligand)

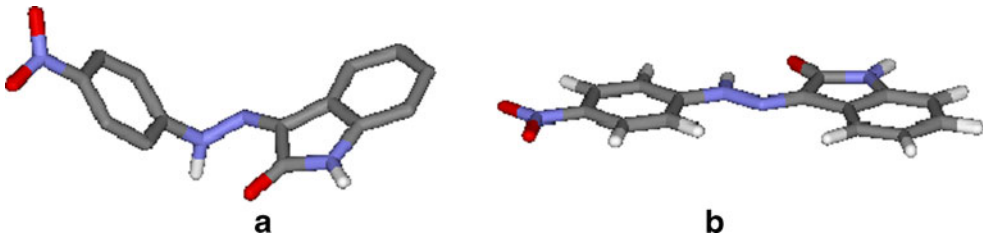

Fig. 5 Conformational structure deviation of 3-(2-(4-nitrophenyl) hydrazono) indolin-2-one in (**a**) docked (VEGFR-2 active site, PDB code: 2OH4) and (**b**) DFT-optimized conformers

Our calculations demonstrated that binding of the ligand to the VEGFR-2 active site led to the perceptible changes in dihedral angles. The rotation around a N11-N13 hydrazine bond afforded a proper orientation to make key H-bonds via nitro group of ligand (Fig. 1). On the other hand, appropriate direction of 4-nitrophenyl functional group may be a direct consequence of twisted N11-N13 bond which provides efficient interactions with Arg1049 and Asn921 residues of the receptor (Fig. 1). This noticeable conformational distortion might be typically exhibited via altered dihedral angles (C5-N11-N13-H14, C5-N11-N13-H15, N11-N13-C15-C16 and N11-N13-C15-C20, Table 5). Moreover, rotation around a C18-N21 bond disturbed coplanarity of nitro substituent with the phenyl ring. The resulted dihedral shifts could be

Table 4 Bond lengths of 3-(2-(4-nitrophenyl) hydrazono) indolin-2-one in the DFT-optimized and docked conformers (VEGFR-2, PDB code: 2OH4)

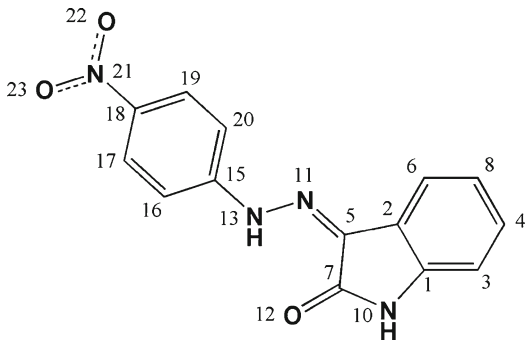

Bond	Bond length (Å)		Bond	Bond length (Å)	
	docked pose	optimized pose		docked pose	optimized pose
C1-C2	1.443	1.413	N11-N13	1.316	1.331
C1-C3	1.390	1.387	N13-H14	1.025	1.025
C1-N10	1.408	1.406	N13-C15	1.410	1.387
C2-C5	1.472	1.456	C15-C16	1.418	1.407
C2-C6	1.382	1.390	C15-C20	1.413	1.408
C3-C4	1.402	1.401	C16-C17	1.386	1.386
C3-H24	1.098	1.0853	C16-H28	1.102	1.082
C4-C8	1.390	1.399	C17-C18	1.404	1.397
C4-H25	1.101	1.086	C17-H29	1.103	1.083
C5-C7	1.523	1.496	C18-C19	1.405	1.396
C5-N11	1.309	1.303	C18-N21	1.482	1.461
C6-C8	1.404	1.398	C19-C20	1.388	1.386
C6-H26	1.100	1.085	C19-H30	1.104	1.082
C7-N10	1.402	1.377	C20-H31	1.104	1.086
C7-O12	1.239	1.233	N21-O22	1.202	1.233
C8-H27	1.100	1.085	N21-O23	1.203	1.233
H9-N10	0.987	1.009	N11-N13	1.316	1.331

Table 5 Dihedral angles of 3-(2-(4-nitrophenyl) hydrazono) indolin-2-one in the DFT-optimized and docked conformers (VEGFR-2, PDB code: 2OH4)

Dihedral angle	Angle (degree)		Dihedral angle	Angle (degree)	
	docked pose	optimized pose		docked pose	optimized pose
C3-C1-C2-C5	179.971	180.0044	C5-C7-N10-C1	0.014	0.0194
C3-C1-C2-C6	−0.165	0.0014	C5-C7-N10-H9	178.103	179.9371
N10-C1-C2-C5	0.138	0.0099	O12-C7-N10-C1	−179.906	−179.9712
N10-C1-C2-C6	−179.999	−179.993	O12-C7-N10-H9	−1.817	−0.0535
C2-C1-C3-C4	0.173	0.0014	C5-N11-N13-H14	−37.520	0.0392
C2-C1-C3-H24	179.986	−179.9965	C5-N11-N13-C15	93.585	179.9962
N10-C1-C3-C4	179.970	179.9946	N11-N13-C15-C16	69.181	0.0152
N10-C1-C3-H24	−0.217	−0.0032	N11-N13-C15-C20	−110.820	180.0098
C2-C1-N10-C7	−0.095	−0.0191	H14-N13-C15-C16	−157.341	179.971
C2-C1-N10-H9	−178.201	−179.9336	H14-N13-C15-C20	22.685	−0.0344
C3-C1-N10-C7	−179.909	179.9869	N13-C15-C16-C17	179.993	179.9928
C3-C1-N10-H9	1.985	0.0724	N13-C15-C16-H28	−0.435	−0.0075
C1-C2-C5-C7	−0.122	0.0017	C20-C15-C16-C17	−0.007	−0.0017
C1-C2-C5-N11	179.917	179.9922	C20-C15-C16-H28	179.556	179.998
C6-C2-C5-C7	−179.964	−179.9948	N13-C15-C20-C19	−179.942	−179.9933
C6-C2-C5-N11	0.076	−0.0043	N13-C15-C20-H31	0.791	0.0116
C1-C2-C6-C8	0.118	−0.0033	C16-C15-C20-C19	0.058	0.0014
C1-C2-C6-H26	−179.951	179.9975	C16-C15-C20-H31	−179.210	−179.9937
C5-C2-C6-C8	179.942	−180.0072	C15-C16-C17-C18	−0.037	−0.0004
C5-C2-C6-H26	−0.127	−0.0064	C15-C16-C17-H29	179.369	179.9997
C1-C3-C4-C8	−0.144	−0.0023	H28-C16-C17-C18	−179.611	−180.0001
C1-C3-C4-H25	179.980	179.9998	H28-C16-C17-H29	−0.205	0
H24-C3-C4-C8	−179.960	179.9956	C16-C17-C18-C19	0.030	0.0029
H24-C3-C4-H25	0.165	−0.0023	C16-C17-C18-N21	−179.999	−179.9973
C3-C4-C8-C6	0.103	0.0005	H29-C17-C18-C19	−179.376	−179.9972
C3-C4-C8-H27	−179.986	−179.9995	H29-C17-C18-N21	0.595	0.0025
H25-C4-C8-C6	179.978	−180.0017	C17-C18-C19-C20	0.021	−0.0032
H25-C4-C8-H27	−0.112	–0.0016	C17-C18-C19-H30	−179.466	180
C2-C5-C7-N10	0.068	−0.0127	N21-C18-C19-C20	−179.950	179.997
C2-C5-C7-O12	179.987	179.9778	N21-C18-C19-H30	0.563	0.0003
N11-C5-C7-N10	179.974	−180.0033	C17-C18-N21-O22	−33.880	−0.0028
N11-C5-C7-O12	−0.055	−0.0128	C17-C18-N21-O23	145.925	−179.999
C2-C5-N11-N13	−179.976	179.984	C19-C18-N21-O22	146.091	−180.0031
C7-C5-N11-N13	0.063	−0.0272	C19-C18-N21-O23	−34.104	0.0007
C2-C6-C8-C4	−0.088	0.0024	C18-C19-C20-C15	−0.0065	0.001
C2-C6-C8-H27	−179.999	−179.9977	C18-C19-C20-H31	179.208	179.9962
H26-C6-C8-C4	179.981	−179.9984	H30-C19-C20-C15	179.424	179.9977
H26-C6-C8-H27	−179.999	0.0015	H30-C19-C20-H31	−1.304	−0.0072

distinguished as distorted N11-N13-C15-C16 and N11-N13-C15-C20 angles (about 35º, Table 5).

Conclusions

In conclusion, our QM-based calculations provided some information on binding energy and binding mode of 3-(2-(4-nitrophenyl) hydrazono) indolin-2-one scaffold in the active site of VEGFR-2. Obtained binding energies could be further evaluated in detail considering basis set superposition errors which is under investigation in combination to MD methods, but at the least point of view, an assisting degree of reliability could be expected for further calculations. Conformational analysis revealed that 3-(2-(4-nitrophenyl) hydrazono) indolin-2-one might not necessarily bind to the

VEGFR-2 active site in its minimum energy conformation. Incorporated hydrazine linker in arylhydrazono indolin-2-one compounds may not participate in key contacts with receptor but at the same time provides an active site oriented pose of the ligand. Moreover the presence of a H-acceptor groups such as nitro moiety in the *para* position of phenyl moiety in the arylhydrazono indolin-2-ones may play an important role in making key H-bonds with VEGFR-2 active site. Induced polarization effects of interacted amino acids on a docked ligand may find their usefulness in assessment of binding patterns on an atomic level. Our calculations demonstrated that a fairly good correlation might be expected between estimated binding energies and induced polarization effects of individual amino acids of VEGFR-2 active site in binding to 3-(2-(4-nitrophenyl) hydrazono) indolin-2-one. Such types of studies may possibly be extended to other biological targets of interest using cognate or biologically evaluated docked ligands, providing some logic inspections prior to synthesis and biological assays of candidate molecules.

Acknowledgments Financial supports of this project by research council of Shiraz University of Medical Sciences are acknowledged.

References

1. Guo YC, Zhongcaoyao F (1986) TLC-UV-spectrophotometric and TLCscanning determination of isatin in leaf of Isatis. Zhongcaoyao 17:8–11
2. Ischia MP, Palumba A, Prota G (1988) Adrenalin oxidation revisited. New products beyond the adrenochrome stage. Tetrahedron 44 (20):6441–6446
3. Binda C, Li M, Hubálek F, Restelli N, Edmondson DE, Mattevi A (2003) Insights into the mode of inhibition of human mitochondrial monoamine oxidase B from high-resolution crystal structures. Proc Natl Acad Sci USA 100:9750–9755
4. Van der Walta EM, Milczekb EM, Malana SF, Edmondsonb DE, Castagnoli N Jr, Bergha JJ, Petzer JP (2009) Inhibition of monoamine oxidase by (E)-styrylisatin analogues. Bioorg Med Chem Lett 19:2509–2513
5. Imam SAV, Varma RS (1975) Isatin-3-anils as excystment and cysticidal agents against Schizopyrenus russelli. Experientia 31 (11):1287–1288
6. Varma RS, Khan IA (1977) Potential biologically active agents. X. Synthesis of 3-arylimino-2-indolinones, and their 1-methyl- and 1-morpholino/piperidinomethyl derivatives as excystment and cysticidal agents against Schizopyrenus russelli. Pol J Pharmacol Pharm 29(5):549–554
7. Khan KM, Khan M, Ali M, Taha M, Rasheed S, Perveen S, Choudhary MI (2009) Synthesis of bis-Schiff bases of isatins and their antiglycation activity. Bioorg Med Chem 17:7795–7801
8. Verma M, Pandeya SN, Singh KN, Stables JP (2004) Anticonvulsant activity of Schiff bases of isatin derivatives. Acta Pharm Turc 54:49–56
9. Smitha S, Pandeya SN, Stables JP, Ganapathy S (2008) Anticonvulsant and sedative-hypnotic activities of N-acetyl / methyl isatin derivatives. Sci Pharm 76:621–636
10. Bhattacharya SK, Chakrabarti S (1998) Dose-related proconvulsant and anticonvulsant activity of isatin, a putative biological factor in rats. Indian J Exp Biol 36:118–121
11. Chohan ZH, Pervez H, Rauf A, Khan KM, Supuran CT (2004) Isatin-derived antibacterial and antifungal compounds and their transition metal complexes. J Enzym Inhib Med Chem 19:417–423
12. Shuttleworth SJN, Gervais DC, Siddiqui MA, Rando RF, Lee N (2000) Parallel synthesis of isatin-based serine protease inhibitors. Bioorg Med Chem Lett 10(22):2501–2504
13. Anderson A (2012) Structure-based functional design of drugs: from target to lead compound. Method Mol Biol 823:359–366
14. Ohacek R, McMartin C, Guida W (1996) The art and practice of structure-based drug design: a molecular modeling perspective. Med Res Rev 16:3–50
15. Leach A (1996) Molecular modelling. Principles and applications, 3rd edn. Addison Wesley, Boston
16. Vedani A, Zbinden P, Snyder J, Greenidge P (1995) Pseudoreceptor modeling: the construction of three-dimensional receptor surrogates. J Am Chem Soc 117:4987–4994
17. Bissantz C, Folkers G, Rognan D (2000) Protein-based virtual screening of chemical databases. 1. Evaluation of different docking/scoring combinations. J Med Chem 43:4759–4767
18. Kubinyi H (1997) QSAR and 3D QSAR in drug design Part 1: methodology. Drug Discov Today 2:457–467
19. Neese F (2011) ORCA – an ab initio, density functional and semiempirical program package. Version 2.8.0, edn. University of Bonn
20. Remko M, Bohác A, Kováčikova L (2011) Molecular structure, pKa, lipophilicity, solubility, absorption, polar surface area, and blood brain barrier penetration of some antiangiogenic agents. Struct Chem 22:635–648
21. Matesic L, Locke JM, Bremner JB, Pyne SG, Skropeta D, Ranson M, Vine KL (2008) N-phenethyl and N-naphthylmethyl isatins and analogues as in vitro cytotoxic agents. Bioorg Med Chem 16:3118–3124
22. Hossain MM, Islam N, Khan R, Islam M (2008) Cytotoxicity study of dimethylisatin and its heterocyclic derivatives. Bangladesh J Pharmacol 2:66–70
23. Vine KL, Locke JM, Ranson M, Pyne SG, Bremner JB (2007) In vitro cytotoxicity evaluation of some substituted isatin derivatives. Bioorg Med Chem 15:931–938
24. Pervez H, Ramzan M, Yaqub M, Khan KM (2011) Synthesis, cytotoxic and phytotoxic effects of some new N4-aryl substituted isatin-3-thiosemicarbazones. Lett Drug Des Discov 8:452–458
25. Sun L, Tran N, Liang C, Tang F, Rice A, Schreck R, Waltz K, Shawver LK, McMahon G, Tang C (1999) Design, synthesis, and evaluations of substituted 3-[(3- or 4-carboxyethylpyrrol-2-yl) methylidenyl] indolin-2-ones as inhibitors of VEGF, FGF, and PDGF receptor tyrosine kinases. J Med Chem 42:5120–5130
26. Phosrithong N, Ungwitayatorn J (2010) Molecular docking study on anticancer activity of plant-derived natural products. Med Chem Res 19:817–835
27. Strawn LM, McMahon G, App H, Schreck R, Kuchler WR, Longhi MP, Hui TH, Tang C, Levitzki A, Gazit A (1996) Flk-1 as a target for tumor growth inhibition. Cancer Res 56:3540–3545
28. Holmes K, Roberts OL, Thomas AM, Cross MJ (2007) Vascular endothelial growth factor receptor-2: structure, function, intracellular signaling and therapeutic inhibition. Cell Signal 19:2003–2012
29. Azizian J, Mohammadi MK, Firuzi O, Razzaghi-asl N, Miri R (2011) Synthesis, biological activity and docking study of some new isatin Schiff base derivatives. Med Chem Res accepted for publication
30. Schafer A, Horn H, Ahlrichs R (1992) Fully optimized contracted Gaussian basis sets for atoms Li to Kr. J Chem Phys 97:2571–2577
31. Morris GM, Huey R, Lindstrom W, Sanner MF, Belew RK, Goodsell DS, Olson AJ (2009) AutoDock4 and AutoDockTools4: automated

docking with selective receptor flexibility. J Comput Chem 30 (16):2785–2791
32. Humphrey W, Dalke A, Schulten K (1996) VMD: visual molecular dynamics. J Mol Graph 14:33–38
33. Wallace AC, Laskowski RA, Thornton JM (1995) Ligplot—a program to generate schematic diagrams of protein ligand interactions. Protein Eng 8:127–134
34. Fogarasi G, Zhou X, Taylor PW, Pulay P (1992) The calculation of ab initio molecular geometries: efficient optimization by natural internal coordinates and empirical correction by offwet forces. J Am Chem Soc 114:8191–8201
35. Mulliken RS (1955) Electronic population analysis on LCAO MO molecular wave functions. IV. Bonding and antibonding in LCAO and valence bond theories. J Chem Phys 23:2343–2346